Journal of
Materials Chemistry B

Materials for biology and medicine

Accepted Manuscript

This article can be cited before page numbers have been issued, to do this please use: M. Said, J. Jing, O. Montigon, N. Collomb, F. Vossier, B. Chovelon, B. El Amine, I. Jeacomine, B. Lemasson, E. L. BARBIER, O. Detante, C. Rome and R. Auzély, *J. Mater. Chem. B*, 2025, DOI: 10.1039/D4TB02722A.

ROYAL SOCIETY OF CHEMISTRY

rsc.li/materials-b

View Article Online
DOI: 10.1039/D4TB02722A

ARTICLE

A T_1 MRI detectable hyaluronic acid hydrogel for *in vivo* tracking after intracerebral injection in stroke

Moustoifa Said,[†ab] Jing Jing,[†b] Olivier Montigon,[ac] Nora Collomb,[c] Frédérique Vossier,[a] Benoît Chovelon,[de] Bayan El Amine,[a] Isabelle Jeacomine,[b] Benjamin Lemasson,[a] Emmanuel Luc Barbier,[ac] Olivier Detante,[af] Claire Rome,[a] Rachel Auzély-Velty[b]*

[a]Univ. Grenoble Alpes, Inserm, U1216, Grenoble Institut Neurosciences, 38000 Grenoble, France
[b]Univ. Grenoble Alpes, Centre de Recherches sur les Macromolécules Végétales (CERMAV-CNRS), 38041 Grenoble, France
[c]Univ. Grenoble Alpes, IRMaGe, Grenoble Institut Neurosciences, 38000 Grenoble, France
[d]Univ. Grenoble-Alpes, Département de Pharmacochimie Moléculaire UMR 5063, 38400 Grenoble, France
[e]CHU de Grenoble-Alpes, Institut de Biologie et Pathologie, 38700 La Tronche, France
[f]CHU Grenoble Alpes, Stroke Unit, Department of Neurology, 38043 Grenoble, France

†M.S. and J.J. contributed equally to this work.

Injectable hydrogels have emerged as a promising strategy for stroke and neurodegenerative diseases, but their effectiveness depends on precise injection, defect filling, and long-term retention at the target site. While MRI can help visualize hydrogels, distinguishing them from fluid-filled spaces, like post-stroke cavity at chronic stage, is challenging due to their high water content and similar MR properties. In this study, a T_1 MRI detectable hyaluronic acid (HA) hydrogel, that is injectable and self-healing, was developed for *in vivo* tracking after intracerebral injection in stroke. The HA hydrogel was functionalized with a thermodynamically stable and kinetically inert Gadolinium(III) complex for monitoring its long-term fate in the brain with T_1-contrast enhanced MRI. The dynamic covalent cross-links based on boronate ester bonds in the hydrogel network ensured precision injection and instantaneous self-healing. The HA network did not induce adverse tissue response and was biocompatible with therapeutic cells (human adipose stromal/stem cells). This labeling strategy enabled accurate tracking of hydrogel distribution and degradation in stroke condition, allowing a better assessment of efficacy and safety. This MRI-visible hydrogel offers significant potential as a scaffold for stem cells, growth factors, and/or drugs, paving the way for more effective treatments for brain disorders.

Introduction

Injectable hydrogels have become a popular scaffolding treatment option for brain disorders, such as stroke, and neurodegenerative diseases.[1-4] Many of these disorders lead to progressive degeneration and/or death of neurons, severe disabilities and have no cure. Due to their high water content and mechanical similarity to native tissue, hydrogels, used alone or loaded with therapeutic agents or cells, provide an effective scaffold for neural tissue growth in areas of brain damage.[5-9] The outstanding advantage of injectable hydrogels is that they can be administered into the target sites *via* minimally invasive procedures, such as stereotactic injections. However, the beneficial effect of injectable hydrogel scaffolds is closely linked to the precision in injection, ability to fill irregular tissue defects and retention at the target site over a long time span. Such information can be achieved by using noninvasive imaging tools to visualize hydrogels.[10] Magnetic resonance imaging (MRI) is ideally suited for this application in both pre-clinical and clinical studies, owing to its safety and penetration depth.[11] Besides, MRI may provide the ability to track in real-time the whole procedure of injection.[12, 13] Yet, while non contrast-based MRI may be used to visualize hydrogels based on intrinsic differences in the MR properties (i.e., T_2 relaxation) between the injected hydrogel and surrounding tissue, it is often hard to distinguish them within the fluid-filled spaces, like post-stroke cavity at chronic stage, due to their high water content.[8] To overcome these issues, hydrogels must be labeled with MRI contrast agents. Gadolinium(III) (Gd(III)) complexes are widely used in clinics to enhance the signal of a T_1-weighted MRI.[14] Several examples of hydrogels incorporating Gd(III)-based contrast agents (GBCAs) have been reported.[11, 15-20] The most straightforward approach for labeling hydrogels with Gd(III) is to covalently conjugate Gd(III)-chelates to the (macro)molecular building blocks used for hydrogel preparation.[10, 21] This strategy offers two advantages. First, it avoids rapid leakage of the GBCA from the hydrogel, which would compromise its specific visualization[11]. Second, it contributes to increasing the T_1-relaxivity (r_1) and so, the contrast[11, 17, 18]. Yet, stability of the Gd(III)-chelate is also a key property to consider when designing Gd(III)-labeled

View Article Online
DOI: 10.1039/D4TB02722A

scaffolds for long-term MRI follow-up. Indeed, Gd(III)-chelate structures have been carefully engineered to tightly bind Gadolinium and prevent the release of this toxic ion.[14, 22] Therefore, the modification of the Gd(III)-chelate structure for its selective grafting on a macromolecular carrier should not affect its stability.

As a primary component of the brain extracellular matrix, hyaluronic acid (HA) is an attractive material for engineering injectable scaffolds for brain repair.[9, 23] Previously, we reported on a new injectable HA hydrogel with dynamic covalent crosslinks, suitable for cell delivery in a minimally invasive process.[24] The hydrogel is formed simply by mixing two solutions of HA partners (HA modified with phenylboronic acid (PBA) and a fructose derivative (Fru)) in physiological conditions. The dynamic covalent crosslinks (boronate ester bonds) in this hydrogel network makes it moldable and able to rapidly recover its normal solid-like state after injection (self-healing). This property suggests that it can be injected with precision to target sites.

In the current study, we modified this dynamic HA hydrogel with a Gd(III)-chelate to investigate its long-term behavior after intracerebral injection *in vivo* (Figure 1). Among Gd(III)-chelates, Gadolinium-1,4,7,10-tetraazacyclododecane-1,4,7,10-tetraacetic acid (GdDOTA) is recognized as one of the most stable GBCAs currently used in MRI.[25, 26] For hydrogel labeling, our strategy was to selectively functionalize one of the HA gel precursors with a GdDOTA-like complex with high thermodynamic stability and kinetic inertness[27]. In this report, the synthesis and characterization of the Gd(III)-labeled HA hydrogel are described. T_1-contrast enhancement due to Gd(III) labeling and prolonged retention of the hydrogel after injection in the brain of healthy rats were then verified by MRI. Moreover, for further uses as scaffolds of stem cells for combined cell therapy in regenerative studies, we assessed *in vitro* biocompatility with human adipose-derived stromal cells (hASCs). Finally, we conducted a proof-of-concept study to demonstrate for the first time the ability to selectively visualize the Gd-labeled hydrogel after intracerebral injection in a rat model of stroke.

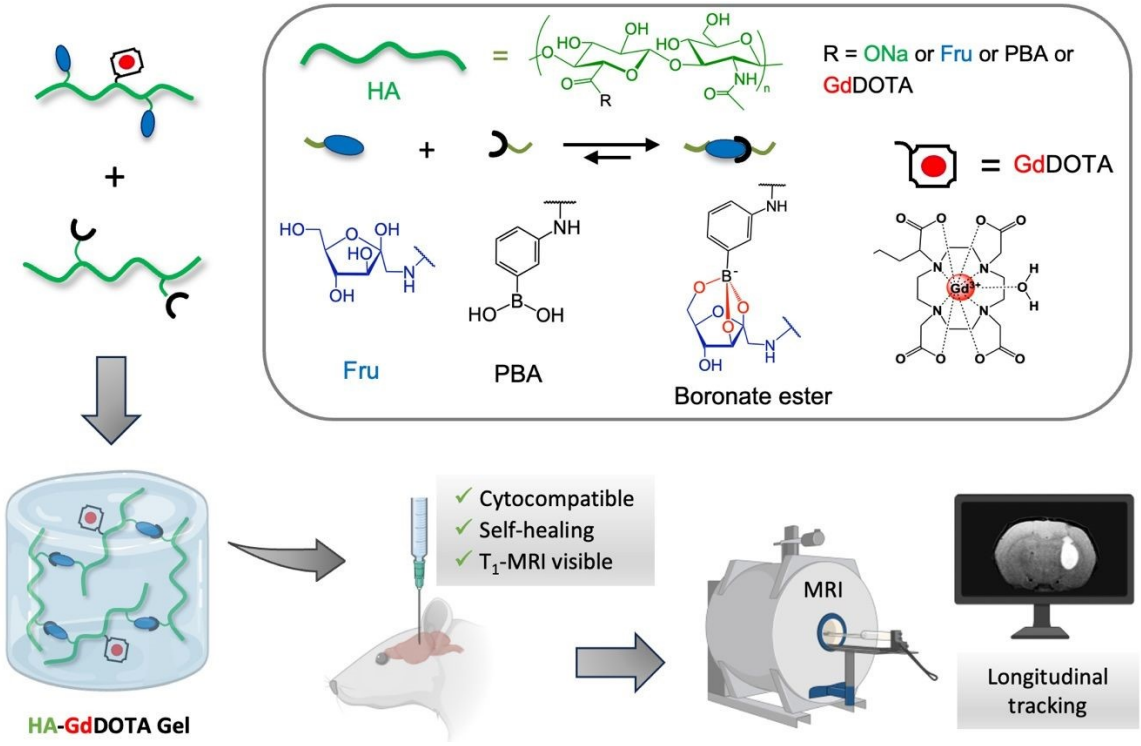

Fig. 1 Schematic presentation of the design and study of the T_1-MRI traceable hyaluronic acid (HA) hydrogel. The hydrogel is produced by mixing solutions of two HA derivatives modified respectively with fructose (Fru) and Gd(III)-chelate (GdDOTA) moieties, and phenylboronic acid (PBA) molecules. The dynamic covalent character of crosslinks (boronate ester bonds) in this hydrogel network makes it injectable and able to self-heal almost instantly. The *in vivo* examination of the HA-GdDOTA hydrogel showed ability to monitor its fate up to 31 days in healthy rat brains and to selectively visualize it in the cerebral lesion in a rat model of ischemic stroke. This figure was created with BioRender.com.

Materials and methods

Materials.

HA, sodium salt, possessing a weight-average molar mass (M_w) of 390 kg/mol was purchased from Contipro France. 1-Amino-1-deoxy-D-fructose hydrochloride (fructosamine) was supplied by Biosynth. 3-Aminophenylboronic acid hemisulfate salt (APBA), adipic acid dihydrazide (ADH), 4-(4,6-dimethoxy-1,3,5-triazin-2-yl)-4-methylmorpholinium chloride (DMTMM), 1-[bis(dimethyl-amino)methylene]-1H-1,2,3-triazolo(4,5-b)pyridinium 3-oxide hexafluoro-phosphate (HATU), 1-ethyl-3-[3-(dimethylamino)propyl] carbodiimide (EDC), phosphate-buffered saline (PBS), 2,2-dimethoxyethylamine, Gadolinium(III) chloride hexahydrate ($GdCl_3 \cdot 6H_2O$), diisopropylethylamine (DIEA), picoline borane

View Article Online
DOI: 10.1039/D4TB02722A

complex ($PicBH_3$), agarose (Reference A9539), and other chemicals were purchased from Sigma-Aldrich and were used without further purification. (*R*)-5-(*tert*-butoxy)-5-oxo-4-(4,7,10-tris(2-(*tert*-butoxy)-2-oxoethyl)-1,4,7,10-tetraaza-cyclododecan-1-yl)pentanoic acid (DOTAGA(O*t*Bu)$_4$) was purchased from CheMaTech (Dijon, France). Therapeutic grade hASCs used in this study were isolated from human adipose tissues of healthy donors (cell stock from French Blood Company, EFS "Etablissement Français du Sang", St Ismier). Platelet lysate and heparin 5000 U/mL, beta fibroblast growth factor (βFGF), Dulbecco's phosphate buffer saline (DPBS), and α-MEM (α-Minimum Essential Media) were purchased from ThermoFisher Life Science.

Methods.

NMR spectroscopy. ^{1}H and ^{13}C spectra were recorded at 25°C or 80°C using a Bruker AVANCE III HD spectrometer operating at 400.13 MHz (^{1}H) and 100.61 MHz (^{13}C). ^{1}H NMR spectra were recorded by applying a 90° tip angle for the excitation pulse, and a 10 s recycle delay for accurate integration of the proton signals. Deuterium oxide (D_2O) and chloroform-d ($CDCl_3$) were obtained from Euriso-top (Saint-Aubin, France). Chemical shifts (δ in ppm) are given relative to external tetramethylsilane (TMS = 0 ppm) and calibration was performed using the signal of the residual protons of the solvent as a secondary reference. All NMR spectra were analyzed with Topspin 4.3.0 software from Bruker.

Determination of free Gd(III) content. The concentration of free Gd(III) was quantified by determination of the ratio of absorbance intensity at λ = 573 nm and λ = 433 nm of a Gd(III)-xylenol orange complex[28] in sodium acetate buffer (50 mM, pH 5.8, 0.60 mM xylenol orange) using a Varian Cary 50 UV-visible spectrophotometer using 1.0 cm quartz cuvettes.

Synthesis of HA-PBA and HA-Fru. HA-PBA and HA-Fru were synthesized by an amide coupling reaction from APBA and fructosamine, respectively.[24, 29] To this end, APBA (0.022 g, 0.12 mmol) or fructosamine (0.024 g, 0.112 mmol) was added to a water/DMF (3/2, v/v) mixture containing DMTMM (0.207 g, 0.75 mmol) and HA (0.300 g, 0.75 mmol) and the pH was adjusted to 6.5 using 0.5 M aqueous NaOH. After stirring for 24 h at room temperature, the HA derivatives were purified by ultrafiltration using deionized water and the products were recovered by freeze-drying. The chemical integrity and purity of the final products were checked by ^{1}H NMR and 2D HSQC NMR (Figure S1 and S2). The degree of substitution (DS, average number of substituting groups per HA disaccharide repeating unit) of the HA-PBA and HA-Fru derivatives were found to be 0.15 from ^{1}H NMR analysis and from the reaction kinetics using the 2,4,6-trinitrobenzene sulfonic acid (TNBS) method[30], respectively.

Synthesis of HA-Fru-ADH. HA-Fru-ADH was prepared by dissolving HA-Fru (0.250 g, 0.593 mmol) in pure water at a concentration of 1 g/L. Adipic acid dihydrazide (0.072 g, 0.415 mmol) was added to this solution. The pH of the reaction was then adjusted to 4.75 using 0.5 M HCl. Next, an aqueous solution of EDC (0.016 g, 0.083 mmol) was added slowly to the mixture. The pH of the reaction mixture was maintained at 4.75 by addition of 0.5 M HCl. The reaction was allowed to proceed at room temperature until no further change in pH was observed (i.e., 4 h). The reaction was stopped by addition of 0.05 M NaOH, raising the pH of reaction mixture to 7.5. A concentrated solution of NaCl was added to obtain a NaCl concentration of 0.5 M. Then, the modified HA was purified by ultrafiltration against water and recovered by freeze-drying. The DS_{ADH} of the HA-Fru-ADH derivatives was found to be 0.05 from ^{1}H NMR analysis (Figure S3).

Synthesis of DOTAGA(O*t*Bu)$_4$-CH(OMe)$_2$. DOTAGA(O*t*Bu)$_4$ (0.050 g, 0.071 mmol) was dissolved in a 9/1 (v/v) mixture of anhydrous CH_2Cl_2/DMF (2.2 mL) under N_2. 2,2-Dimethoxyethylamine (0.009 g, 0.086 mmol), HATU (0.032 g, 0.086 mmol), and DIEA (0.037 mL, 0.214 mmol) were added and the mixture was stirred for 4 h at room temperature. Then, the organic phase was evaporated and the oily residue was re-dissolved in ethyl acetate (15 mL). The organic phase was washed with 1 N HCl (2 x 5 mL), water (2 x 5 mL) and brine (2 x 5 mL) and dried over Na_2SO_4. After evaporation of the solvent under reduced pressure, the product was recovered as a glassy solid (0.030 g, 53 % yield).

^{1}H NMR ($CDCl_3$) 400 MHz δ_H = 6.02 (1H, t, N*H*CO), 4.42 (1H, t, C*H*(OCH$_3$)$_2$), 3.53 (m, 1H, C*H*N), 3.50-3.25 (8H, m, C*H*$_2$COOtBu, CONHC*H*$_2$), 3.39 (6H, s, CH(OC*H*$_3$)$_2$), 3.06-2.70 and 2.68-2.17 (16H, m, NC*H*$_2$-C*H*$_2$N), 2.16-1.91 (3H, m, C*H*$_b$H$_b$,C*H*$_a$H$_a$,CONH), 1.84 (1H, m, CH$_b$*H*$_b$,CH$_a$H$_a$,CONH), 1.49, 1.44 (36H, s, C(C*H*$_3$)$_3$).

Synthesis of DOTAGA-CHO. DOTAGA(O*t*Bu)$_4$-CH(OMe)$_2$ (0.030 g, 0.038 mmol) was dissolved in dichloromethane (0.5 mL). Trifluoroacetic acid (1.5 mL) was added to the solution and the mixture was stirred for 19 h at room temperature. The solution was evaporated under vacuum, affording the desired product as a glassy solid in 99 % yield.

^{1}H NMR (D_2O, pD 1) 400 MHz δ_H = 5.10 (1H, t, C*H*(OH)$_2$), 4.25-2.85 (m, 25H, C*H*N, C*H*$_2$COOH, CONHC*H*$_2$, NC*H*$_2$-C*H*$_2$N), 2.60 (2H, m, C*H*$_2$CONH), 2.04 (2H, m, C*H*$_2$CH$_2$CONH).

Synthesis of GdDOTAGA-CHO. The ligand DOTAGA-CHO (0.029 g, 0.063 mmol) was dissolved in water at pH 5 (2 mL) at room temperature. $GdCl_3 \cdot 6H_2O$ (0.066 g, 0.25 mmol) was dissolved in water (1 mL) and added to the solution drop by drop (~ 50-80 µL every 20 min), while maintaining the pH at 5 with 1 M sodium hydroxide and the reaction medium at 40°C. The reaction was stirred for 24 h at 40°C. We used the xylenol orange test to confirm that complex was fully formed. The resulting Gd-DOTA-like complex was then used without further purification for coupling with HA-Fru-ADH.

Synthesis of HA-Fru-GdDOTA. To a solution of HA-Fru-ADH (0.100 g, 0.233 mmol) in a water/EtOH (5/3, v/v) mixture (40 mL), GdDOTAGA-CHO (0.009 g, 0.017 mmol) was added, followed by $PicBH_3$ (0.012 g, 0.116 mmol). The pH of the solution was then adjusted to 5.1 by the dropwise addition of a 0.1 M aqueous HCl solution. After stirring for 40 h at room temperature, the pH of the reaction was then adjusted to 7.5 with aqueous 0.1 M NaOH and the product was purified by ultrafiltration, and recovered by freeze-drying. The total amount of incorporated Gd(III) complex in the final

View Article Online
DOI: 10.1039/D4TB02722A

product was 3.5 % (mol/mol of disaccharide units), which was determined by inductively coupled-mass spectrometry (ICP-MS, Perkin Elmer NexION 2000, Waltham, MA, USA).

Preparation of the Gd-labeled and unlabeled HA hydrogels. Hydrogels were prepared by mixing solutions of HA-PBA, HA-Fru-GdDOTA and/or HA-Fru in DPBS (pH 7.4) with a boronic acid/fructose molar ratio of 1/1, using a double-barrel syringe equipped with an extruder (MEDMIX, Switzerland). The concentrations of HA derivatives used to prepare hydrogel formulations for *in vitro* MR imaging, rheological analyses, injection tests and *in vivo* experiments are given in Table 1.

Tableau 1. Composition of hydrogel formulations

Hydrogel	[HA derivatives] (g/L)			[Gd^{3+}] (mM)	Total polymer concentration (C_p) (g/L)	[HA_{eq}] (g/L)
	HA-PBA	HA-Fru-GdDOTA	HA-Fru			
HA-ref[a]	5.95	0	6.05	0	12.00	11.5
HA-GdDOTA[a]	6.63	7.90	0	0.61	14.53	13.4
HA-ref[b]	8.05	0	7.70	0	15.75	15.5
HA-GdDOTA[b]	8.05	8.43	0.52	0.65	17.00	15.5
	8.05	3.37	5.60	0.26	17.02	15.5
	8.05	1.69	7.30	0.13	17.04	15.5

[a]Formulations prepared for rheological analyses, injection tests, *in vitro* cell viability assays and *in vivo* experiments. [b]Formulations prepared for *in vitro* MR imaging to investigate the dose effect of Gd. [HA_{eq}] corresponds to the concentration in HA disaccharide repeating units.

Agarose gel preparation and injection tests*:* Agarose gels were prepared by solubilizing agarose (300 mg) in 50 mL of DPBS (pH 7.4) under stirring at 95 °C for 10 min. The agarose solution was then poured in an Eppendorf® tube and the sample was kept at 4 °C for 24 h before the injection tests. The latter were carried out with a TJ-1A syringe pump controller (Aniphy, USA), at a rate of 5 µL/min.

Rheological measurements. Oscillatory shear experiments were performed with a cone-plate rheometer (AR2000Ex from TA Instruments). The cone used for viscoelastic samples has a diameter of 2 cm and an angle of 4°. To prevent water evaporation, the measuring system was surrounded with a low-viscosity silicon oil (50 mPa.s) carefully added to the edges of the cone. Oscillatory frequency sweep (0.01-10 Hz) experiments were performed within the linear viscoelastic range (strain fixed at 5 %) to determine the frequency dependence of the storage (*G'*) and loss (*G"*) moduli. Oscillatory amplitude sweep experiments at 1 Hz were used to determine the linear-viscoelastic range of the hydrogel networks and to derive the yield stress. They were immediately followed by time sweep experiments at 1 Hz and a strain of 5 % (linear viscoelastic region) to monitor the recovery of the rheological moduli.

Cell viability study. The clinical grade human ASCs used in this study were obtained from Cell Therapy and Engineering Unit of EFS Auvergne Rhone Alps (Saint-Ismier, France). The cells were thawed, expanded (using a seeding density of 2×10^3 viable cells/cm^2) on tissue culture flasks (FisherScientific), and maintained in Minimum Essential Media-alpha (1X) (MEM-Alpha, Gibco), supplemented with 3% Human Platelet Lysate and 1% heparin 5000 U/mL with 5% CO_2 at 37 °C. When the cells reached > 90% confluence, the hASCs were trypsinized, centrifuged for 10 minutes at 1250 rpm at room temperature and re-suspended into a growth media for cell counting. An aliquot of growth media containing hASCs was taken to obtain a final density of encapsulated cells in the hydrogels of 5×10^5 cells/mL. hASCs were pelleted and resuspended in a solution of the HA-Fru-GdDOTA derivative in DPBS (pH 7.4). The HA-PBA solution was transferred to Transwell® cell culture inserts (0.4 µm porous membrane; Corning®, US) contained in 24-well plates. The cell-laden solution of HA-Fru-GdDOTA in DPBS was quickly transferred individually to the insert then mixed with the HA-PBA to form the cell-embedded Gd-labeled HA hydrogel. The cell-laden HA-ref hydrogel based on HA-PBA and HA-Fru with a final density of 5×10^5 cells/mL was prepared following the same procedure. The cell-laden hydrogels were supplemented with standard growth media and incubated for evaluating cell viability over 3 and 7 days at 37°C - 5 % CO_2. For each hydrogel condition, the experiment was carried out in triplicate (n=3) and with three different hASCs batches, at different times. To characterize viability, hASC-laden hydrogels were cultured in a solution of DPBS supplemented with calcein acetoxymethyl and propidium iodide solution for 15 min at 37°C (Live/Dead Cell Double staining kit, Sigma-Aldrich). The gels were washed with DPBS and imaged with an epifluorescence microscope (ZEISS Axiovert 200M) equipped with a CoolSnap HQ^2 camera using MetaMorph 3.5 imaging software. Images of cells encapsulated in the hydrogels were acquired using a 10X objective. 2D images were captured from 10 random fields of view for each sample. Cells labeled by green fluorescent and red fluorescent reactive dyes (live cells and dead cells, respectively) were counted using Image analysis software, ImageJ (ImageJ v1.43, Bethesda, Maryland, USA). For each condition, the experiments were independently conducted in triplicate on three separate occasions.

Animal care. All animal procedures were approved by the Ethical Committee on Animal Experiments of GIN (1098, APAFIS agreement #2015040716522967) and conducted in accordance with the European regulations for animal use (EEC Council Directive 2010/63/EU, OJ L 276, Oct. 20, 2010).

View Article Online
DOI: 10.1039/D4TB02722A

An acclimation period of at least 7 days was observed before the start of the study. Because our *in vivo* and *ex vivo* studies aimed to provide a proof-of-concept of imaging feasibility (and not a treatment effect), we did not calculate a priori sample size, randomize animals in treatment groups nor blind allocation and analysis. All animals were included in the studies. Nine adult male Sprague-Dawley rats (age at reception: 6-7 weeks, body weight: 250-300 g) were purchased from Charles River (Saint-Berthevin, France). The animals were housed in a temperature- and humidity-controlled environment (21 ± 3°C), with a 12-hour light-dark cycle. They had free access to standard show and water and nest material according to the involved animal welfare units. During experimental procedures, rats were anesthetized with isoflurane (3 % for induction, 2% for maintenance, in 0.7 L/min O_2)[31] using an anaesthesia compact module (Minerve, Esternay, France). Then, animals were mounted in a stereotaxic apparatus (D. Kopf Instruments) and pre-medicated with methylprednisolone (0.4 mg/kg). Body temperature was maintained 37°C with care.

For *in vivo* imaging, anesthesia was induced and maintained in the same way as during the surgery. The animals were placed in an MRI-compatible rats cradle. Respiratory rate and body temperature were maintained respectively around 60 breaths per min and 37°C with care.

At the end of the experimental procedures, the rats recovered under supervision in a warmed room and were closely observed until they fully regained consciousness, ensuring their well-being and recovery.

Hydrogel injection in healthy rat brain. Under general anesthesia, after local intradermal injection of 0.1 mL of lidocaine 2%, and scalp incision, a small hole was drilled (1 mm diameter) under saline cooling. Lubricant ophthalmic gel was applied on both eyes to prevent ocular dehydration, and the surgical site was shaved and disinfected with antiseptic solution (i.e. 10 % iodopovidone). All rats had received one intracerebral injection in each of their two hemispheres (stereotaxic coordinates from bregma (mm): anterior-posterior (AP), 0; medium-lateral (ML), ± 3.0; dorsal-ventral (DV), 6.0 from dura) using a 10 µL microsyringe with a 26G (0.4 mm) needle, beveled 40° (Hamilton, 701 N, ThermoFischer, USA). The injection speed was calibrated at 5 µL/min. Treatment consisted in HA-ref hydrogel (10 µL, n=9 injections) and HA-GdDOTA hydrogel (10 µL, n=9 injections). After injection, the needle was staying in place until 2 min before withdrawal of the 10 µL-precise syringe to limit the backflow. The burr hole was sealed, skin resewn and rats were allowed to recover in their home cages in a warmed room.

Induction of focal ischemic lesion in rats and hydrogel implantation. Focal ischemic stroke was modeled in the rat by the striatal injection of 2 µL of a solution of the mitochondrial toxin malonate (3 M in PBS, pH 7.4).[32] Rats (n=4) were anesthetized with isoflurane (3% for induction, 2% for maintenance, in 0.7 L/min O_2), mounted in a stereotaxic frame and pre-medicated with methylprednisolone (0.4 mg/kg). After local intradermal injection of 0.1 mL of lidocaine 2%, and scalp incision, a small hole was drilled (1 mm diameter) under saline cooling. Malonate was injected using a 10 µL microsyringe with a 26G (0.4 mm) needle, beveled 40° (Hamilton, 701 N, ThermoFischer, USA) connected to a micro-pump (TJ-1A Syringe Pump Controller, Aniphy, USA) with an injection rate of 0.33 µL/min). The stereotaxic coordinates targeted, were: AP, -1.5 mm; ML, +3.4 mm; DV, -7 mm (adapted from Cirillo et al.[32]). After the injection, the needle was left in place for additional 2 min to avoid backflow. The burr hole was sealed, skin resewn and rats were allowed to recover in their home cages. Following malonate injection, on the same day, live brain imaging was performed to monitor the striatal injections of malonate by MRI on a preclinical 4.7T MR-system (Bruker BioSpec 47/40, Avance III, Germany). Six days after malonate injection, all rats underwent live brain imaging to characterize the ischemic lesion (presence, location and volume), and to determine its stereotaxic coordinates from MR images. Lesion volumes ranged from 10 to 43 mm^3 from analysis of the T_2-weighted MR images. These values are in the range of lesion volumes previously measured on larger groups of rats (5-60 mm^3, n = 20) at 7-days post-stroke in our laboratory. After exclusion of one animal with no lesion, the remaining 3 rats received intracerebral injection of the HA-GdDOTA hydrogel according to the stereotaxic coordinates of the ischemic site for each rat following the hydrogel injection procedure described above (10 µL, injection rate of 5 µL/min with an additional pause of 2 min before the withdrawing of the needle).

MR imaging and measurements of relaxation times. MRI measurements on hydrogel phantoms and on animals were performed on a 4.7T MR-system (Bruker BioSpec 47/40, Avance III, Germany) using a quadrate 1H volume coil with a diameter of 86 mm. Images of solutions of HA-Fru-GdDOTA and hydrogels in DPBS at 25°C were measured at room temperature directly after preparation, inside Eppendorf® tubes that were placed in a custom-made sample holder. T_1W images were acquired by using a T_1-FLASH sequence (TR = 300 ms, TE = 3.5 ms, flip angle = 40°, bandwidth = 34,091 kHz, resolution between 0.117 x 0.117 x 1.0 (rat) and 0.156 x 0.156 x 1.0 (tubes) mm^3). T_2W images were acquired by using a T_2-TurboRARE sequence (TR = 2200 ms, TE = 36 ms, flip angle = 180°, bandwidth = 28,846 kHz, resolution = 0.117 x 0.117 x 1.0 (rat) and 0.312 x 0.312 x 1.0 (tubes) mm^3). Multi-repetition time (TR) rapid acquisition with relaxation enhancement (RARE) sequence was applied for each sample to measure the T_1 (longitudinal relaxation time) saturation recovery. The scan parameters were: echo time (TE) = 5.89 ms; 24 TRs from 80 to 7000 ms; 1 slice with a thickness of 1.0 mm, image resolution = 0.46 × 0.46 mm and RARE factor = 2. The total scan time was 19 min, 42 s.

For T_2 (transverse relaxation time) signal decay estimation, multi-slice and multi-echo (MSME) spin echo sequence was used for each sample with 96 TEs (i.e., 5–480 ms increased by 5 ms each). Other scan parameters were TR = 4000 ms, 1 slice with a thickness of 1 mm, and image resolution = 0.46 × 0.46 mm. The total data acquisition time was 8 min 32 s.

View Article Online
DOI: 10.1039/D4TB02722A

Image processing and analysis.

The maps of relaxation time (T_1 and T_2) were performed using a program written in Python and the relaxometry parameters were estimated by fitting the data using a non-linear curve fit according to the Levenberg-Marquardt algorithm. The T_1 saturation recovery curve was fit at different TRs using the following equation: $M_z\,(TR) = M_0 \times (1\text{-}\exp\,[-TR / T_1]) + C$.

The T_2 signal decay was estimated at different TEs using a mono-exponential model :

$M_z\,(TE) = M_0 \times \exp\,(-TE / T_2) + C$ with the exclusion of the first TE point for accurate fitting[33].

The specific relaxivities (r_1 and r_2) were calculated from the measured T_1 and T_2 values based on the following equations where $T_{1(0)}$ and $T_{2(0)}$ are the T_1 and T_2 values without contrast agent:

$$1/T_1 = 1/T_{1(0)} + r_1\,[Gd^{3+}] \quad (1)$$

$$1/T_2 = 1/T_{2(0)} + r_2\,[Gd^{3+}] \quad (2)$$

The volume and mean T_1 measurements were carried out with ImageJ by tracing ROIs 'left' and 'right'. T_2-weighted and T_1-weighted images were used for volume measurement, and T_1 maps for mean T_1.

Laser-Induced Breakdown Spectroscopy. LIBS elemental imaging was performed at room temperature on rat brain cryosections (10 µm-thick) mounted onto plastic slides. The samples were analyzed to detect and localize sodium and gadolinium in the biomedical samples. The LIBS instrument for this experiment is a high performance imager (ELM-XS, Ablatom, France) based on microLIBS setup dedicated to biomedical samples. The laser used was a Nd:YAG operating at 100 Hz repetition rate with an laser energy of 1 mJ Images were acquired with a 40 µm lateral spatial resolution, using a laser scan with a single laser shot measurement per site. The light emitted by the plasma was collected and analyzed by a Czerny-Turner spectrometer equipped with an intensified charge-coupled device camera. With this configuration, the gadolinium and sodium were simultaneously and well detected respectively at Gd (I) 342 nm and Na (I) 330 nm. On each pixel of tissue section image, the net intensity of a given emission line was obtained by subtracting the emission background from the line intensity. LIBS images of single thin sections were 420 x 300 pixels wide and were acquired in 20 min. The experiments and the data treatment were performed by Ablatom S.A.S (Lyon, France).

Histological observation. After MRI analyses, the hydrogel-bearing rats were euthanized *via* decapitation. Their brains were promptly removed, frozen at -40°C, and subsequently stored at -80°C for histological analysis. The frozen brains were sectioned using a cryotome to obtain coronal slices of 10 µm thickness. Haematoxylin and eosin (H&E), cresyl violet (CV), GFAP and Collagen-IV (ColIV) stainings were performed at the CIQLE (Quantitative Imaging Center of East Lyon, https://ciqle.univ-lyon1.fr/).

For immunohistochemistry, sections were fixed in paraformaldehyde (Fluka Chemie AG, Buchs, Switzerland). The brain sections were then incubated overnight at 4°C with rabbit anti-GFAP (1:1000, DAKO, 70334) or rabbit anti-Iba1 (1:500, Abcam, ab108539) antibodies. Subsequently, sections were incubated with goat anti-rabbit (1:1000, Invitrogen, A11008) or donkey anti-mouse (1:1000, Thermo Fisher, A31540) secondary antibodies. After rinsing in PBS-Tween 0.1%, coverslips were applied to the slides with the nuclear marker DAPI (Thermo Fisher).

Images were digitized using the Axioscan scanner (Zeiss, Oberkochen, Germany) at the PIC-GIN platform (https://neurosciences.univ-grenoble-alpes.fr/en/research/technological-platforms/pic-gin-platform) and analyzed using ZEN 3.10 software (Zeiss, Oberkochen, Germany).

Results

1. Synthesis of the HA-GdDOTA hydrogel precursors

Our strategy for the synthesis of the HA-GdDOTA hydrogel relied on the modification of one of its precursors, HA-Fru, with a GdDOTA-like complex (Figure 2). HA-Fru was preferably chosen as it gives less viscous solutions than HA-PBA. Both HA-Fru and HA-BPA were prepared by reacting HA with fructosamine and 3-aminophenylboronic acid, respectively, *via* amide bond formation using DMTMM as a condensing agent (Figure 2).[24, 29] Using DMTMM/HA and amine/HA molar ratios of 1 and 0.16-0.15, respectively, we obtained HA derivatives with a DS of 0.15. The final amount of PBA modification was confirmed by ^{1}H NMR (Figure S1, Supporting Information). In the case of HA-Fru, the DS was estimated from the reaction kinetics performed using TNBS to quantify the free primary amines in the reaction medium as a function of time[24, 29] and successful grafting was confirmed by 2D HSQC NMR analysis (Figure S2).

DOTA can be grafted to targeting moieties through amide bond formation with one of its carboxylic acids.[14, 34] However, the change of a coordinating carboxylate to an amide reduces the stability of the GdDOTA complex.[34, 35] To overcome this problem, we selected the DOTAGA (GA= glutaric acid) derivative as a Gd(III)-chelating agent as it contains four coordinating acetate pendant arms even after its conjugation to a biomolecule thanks to the GA side chain.[27, 36] The GdDOTA-like complex was thus expected to be highly stable and extremely inert to gadolinium loss after conjugation to HA-Fru. As HA-Fru also contains carboxylic acid groups, we employed a reductive amination strategy for the chemoselective coupling of the GdDOTA-like complex, where hydrazide groups introduced on HA-Fru can selectively react with GdDOTAGA modified with an aldehyde function (referred to as "GdDOTAGA-CHO"). Of note, Gd(III) was first complexed with modified DOTAGA-CHO prior to conjugation to HA-Fru to avoid competitive binding of Gd(III) to the numerous carboxylate groups of the HA backbone conjugate[37]. As interaction between HA carboxylates and Gd(III) ions are weak, it became important to prevent release of these highly toxic ions after *in vivo* implantation due to undesired complexation with the HA backbone.

HA-Fru modified with hydrazide groups was synthesized by reaction of HA-Fru with ADH in the presence of EDC following

View Article Online
DOI: 10.1039/D4TB02722A

conditions described in a previous work[38] (ADH/HA and EDC/HA molar ratios of 0.7 and 0.14). The DS_{ADH} of the HA-Fru-ADH conjugate was controlled by the amount of EDC used and, under such conditions, it was found to be 0.05 from ^{1}H NMR analysis (Figure S3).

GdDOTAGA-CHO, was synthesized in three steps starting from the *tert*-butyl ester protected DOTAGA intermediate (DOTAGA(O*t*Bu)$_4$, Scheme S1). The free carboxylic acid was reacted with 2,2-dimethoxyethylamine in the presence of HATU and DIEA, followed by treatment with trifluoroacetic acid, to afford the TFA salt of the desired deprotected product in 99 % yield. The crude DOTAGA-CHO ligand was then chelated with $GdCl_3$ ($GdCl_3$/DOTAGA-CHO molar ratio of 0.9) at pH 5 prior to coupling with HA-Fru-ADH. The absence of free Gd(III) in the product was confirmed with the xylenol orange test[28]. The GdDOTAGA-CHO chelate was then coupled with HA-Fru-ADH in a water/ethanol mixture at pH 5.1, in the presence of picoline borane complex as a reducing agent, affording HA-Fru-GdDOTA. This procedure was previously shown to occur cleanly to give the desired product in very high yields.[38] After purification by ultrafiltration, the ICP-MS results demonstrated that the content of Gd(III) in HA-Fru-GdDOTA was 4 % as mol percentage of repeating disaccharide unit. Structural characterization of HA-Fru-GdDOTA by NMR was impossible as it showed a broad unresolved spectrum due to enhanced relaxation caused by Gd(III) labeling (Figure S4).

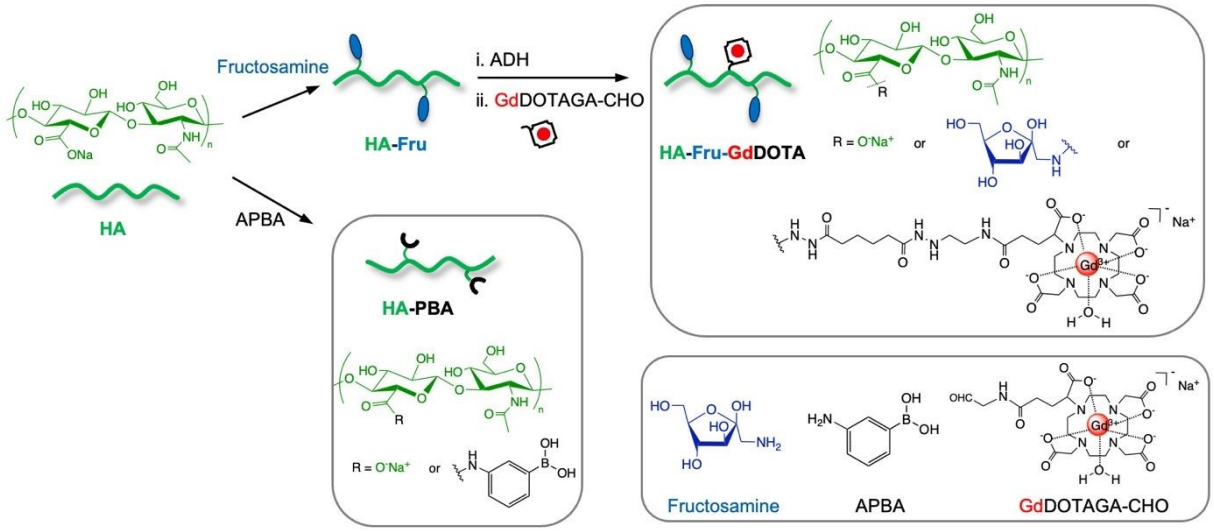

Fig. 2 Synthesis of the HA hydrogel precursors. Fructosamine and 3-aminophenylboronic acid (APBA) are introduced on HA by an amidation reaction to yield HA-Fru and HA-PBA, respectively. The Gd(III) chelate modified with an aldehyde function (GdDOTAGA-CHO) is covalently grafted on HA-Fru functionalized with adipic acid dihydrazide (ADH) by a reductive amination reaction to yield HA-Fru-GdDOTA.

2. Hydrogel preparation, rheological characterization, and cytocompatibility studies

HA-Fru-GdDOTA and HA-PBA were easily solubilized in DPBS (pH 7.4) and quickly crosslinked to form a hydrogel (total polymer concentration, C_p = 14.5 g/L), when mixed using a dual-barrel syringe.

The dynamic mechanical properties of the HA-GdDOTA network crosslinked by dynamic boronate ester bonds were analyzed by rheometry using a frequency sweep test (Figure 3). As shown in Figure 3A, the network exhibits an elastic behavior ($G' > G''$) within the frequency window explored, similar to the non-labeled HA hydrogel (referred to as "HA-ref hydrogel") prepared by mixing HA-Fru and HA-PBA (C_p = 12 g/L). The storage moduli (G') at 1.0 Hz of both HA-GdDOTA and HA-ref hydrogels (Figure 3B) fell into the range of brain tissue stiffness (i.e., 200-2000 Pa),[39] indicating their potential for brain applications. The dynamic covalent nature of the crosslinks should impart the networks with the ability to be extruded under an application of shear (needle injection) and rapidly recover the gel state when the applied stress is removed (self-healing ability). To assess this property, the hydrogel networks were subjected to oscillatory shear deformations with increasing oscillatory strain amplitudes until network disruption, followed by a low strain deformation allowing them to recover. The networks were found to self-heal immediately after network rupture at high strains, showing a recovery of their initial rheological properties (Figure 3C). Finally, injection tests of the HA networks in an agarose brain phantom[40, 41] were carried out to verify their suitability for intracerebral injection. To this end, the hydrogels (10 µL) were injected using a Hamilton syringe with a 26G needle and a stereotaxic injector pump, similar to conditions used for intracerebral injections in rats. As illustrated in Figure 3D, the HA-GdDOTA hydrogel stained in blue (methylene blue) could be injected with precision in the agarose brain phantom, at a rate of 5 µL/min and re-formed immediately into a cohesive hydrogel network. Preliminary injectability studies, in which the G' modulus of the hydrogel was varied by adjusting the concentration of hydrogel precursors, demonstrated that formulations exhibiting a G' at 1 Hz greater than 450 Pa lost their ability to self-heal in the agarose brain phantom (data not shown). A similar behavior was observed with the HA-ref network, indicating that both HA hydrogel formulations are suitable for minimally-invasive injection into brain tissue.

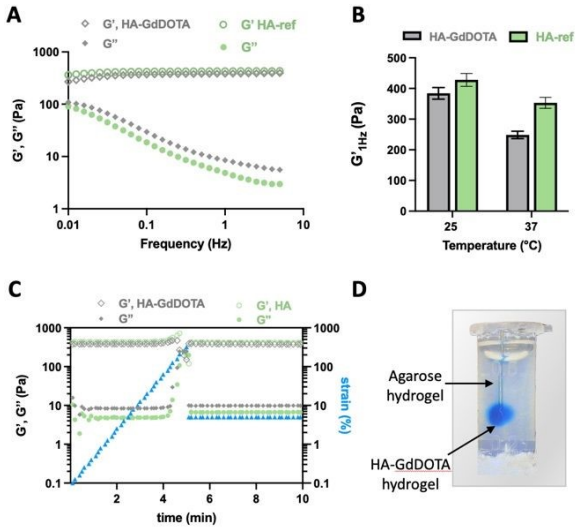

Fig. 3 Rheological behavior and injectability of HA-GdDOTA and HA-ref hydrogels. A) Frequency dependence of the storage modulus (*G'*) and loss modulus (*G''*) measured with 5 % strain at 25 °C. B) *G'* values at 1 Hz of the Gd-labeled and unlabeled hydrogels at room and body temperature. C) Variation of *G'* and *G''* when increasing strain values to 320 % (hydrogel disruption), followed by reducing the strain to a constant value of 5 % (linear viscoelastic region). D) Photo of injection the HA-GdDOTA hydrogel in an agarose brain phantom through a 26G (0.46 mm diameter) needle (methylene blue was added to color the hydrogel for visualization only).

Cell compatibility is essential for the Gd-labeled HA hydrogel to be applicable *in vivo*. To evaluate the cytocompatibility, we encapsulated hASCs within the hydrogel and investigated their viability for 3 and 7 days. The HA-ref hydrogel was used as a reference to assess the impact of the grafted GdDOTA-like moieties. hASCs were used because they are attractive cells for therapeutic applications and have already been evaluated in Phase I and II clinical trials for ischemic stroke[31]. The two HA scaffolds showed high cytocompatibility over the course of 7 days of cell culture (>80% of cell viability, Figure 4). Moreover, no statistically significant change in cell viability was observed for the cells embedded in the HA-GdDOTA hydrogel compared to the cells in the HA-ref hydrogel, indicating that the Gd-labeling has no obvious cytotoxic effect. Given the strong toxicity of free gadolinium, these data indicate high stability of the Gd(III) chelate.

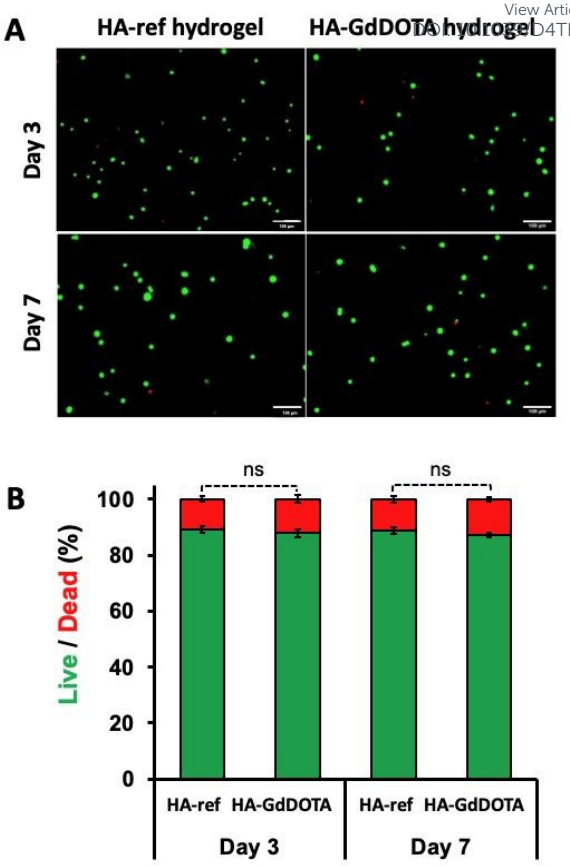

Fig. 4 Cytocompatibility of the HA-GdDOTA hydrogel ([Gd^{3+}] = 0.61 mM) in comparison to that of the HA-ref scaffold after 3 and 7 days of 3D cell culture of human adipose derived stromal cells (hASCs). A) 2D microscopy images (fluorescence, scale bar = 200 µm) of Live/Dead (green/red) staining of hASCs encapsulated in the HA-ref and HA-GdDOTA hydrogels after 3 and 7 days of culture. Quantification of cell viability from Live/Dead assay, represented as mean ± SD (n = 3). Statistical analysis used the one-way analysis of variance (ANOVA); ns: not significant.

3. *In vitro* MR imaging

The T_1 and T_2 images of solutions of the Gd-labeled HA-Fru partner and the resulting HA-GdDOTA hydrogel in DPBS at different concentrations of the HA-Fru-GdDOTA polymer (i.e. Gd(III) concentration) are shown in Figure 5A,B. To prepare the different hydrogel formulations, HA-Fru-GdDOTA was replaced by non-labeled HA-Fru to maintain a constant crosslinking density (See Table 1, Experimental section). For comparison, the commercially available free contrast agent Dotarem® (GdDOTA) was physically incorporated in the HA-ref hydrogel at the highest Gd(III) concentration tested (i.e. 0.65 mM). MR images were acquired on a 4.7T pre-clinical MRI scanner.

As expected, the signal intensity in the T_1 images increased with increasing the Gd(III) concentrations for the HA-Fru-GdDOTA polymer (Figure 5A) and the HA-GdDOTA hydrogel (Figure 5B). Moreover, both T_1 and T_2 values were shortened with increasing Gd(III) concentration resulting in $r_1 \approx 6.7$ mM^{-1} s^{-1} and $r_2 \approx 25$ mM^{-1} s^{-1} for the HA-Fru-GdDOTA alone in DPBS and, $r_1 \approx 7.4$ mM^{-1} s^{-1} and $r_2 \approx 34$ mM^{-1} s^{-1} for the HA-GdDOTA hydrogel (Figure 5C,D). It is also worthy of note that the measured $r_1 \approx 4.4$ mM^{-1} s^{-1} for Dotarem® is well in line with values reported in the literature.[22, 42, 43] We can notice

View Article Online
DOI: 10.1039/D4TB02722A

an increase in the relaxivity r_1 of the Gd(III)-chelate when the chelate is attached to HA compared to commercial Dotarem® physically mixed in hydrogel, which is due to decrease in molecular tumbling. The crosslinking of HA chains has also a slight effect on the relaxivity r_1 of the Gd(III)-chelate grafted on the polysaccharide as can be noticed from the value increasing from 6.7 to 7.4 mM^{-1} s^{-1}. These results are in line with previous reports showing that incorporation of a Gd(III) chelate in cross-linked HA networks resulted in an increase of the relaxivity.[44] This was related to the altered hydration mechanism of the contrast agent confined within the HA network. It should be noted that as the hydrogel has a high-water content, the T_2-weighted signal of the HA network is easily identified with or without Gd labeling (Figure 5A,B).

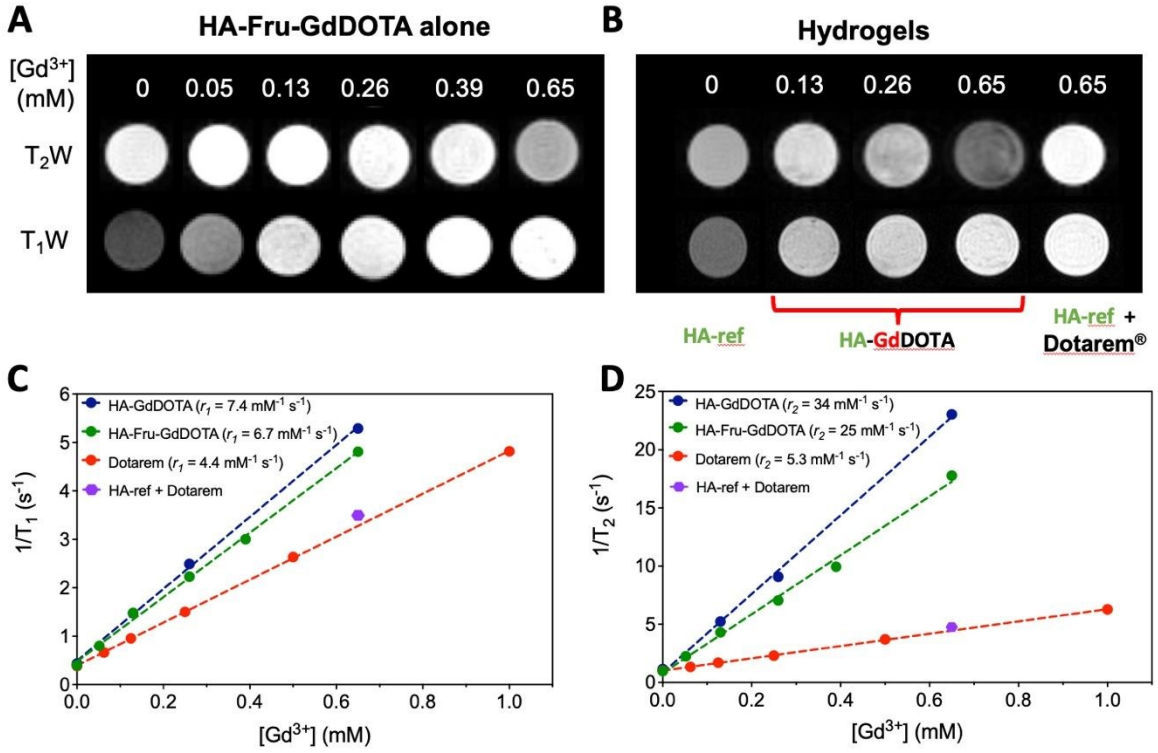

Fig. 5 MR images and relaxation rates at 4.7T of phantoms of HA-Fru-GdDOTA solutions and HA hydrogels. T_1W and T_2W MR images of A) solutions of HA-Fru-GdDOTA and B) hydrogels at different Gd(III) concentrations in DPBS at pH 7.4. C) $1/T_1$ and D) $1/T_2$ relaxation rates of HA-GdDOTA hydrogels, HA-Fru-GdDOTA solutions, commercial Dotarem® solutions, and HA-ref + Dotarem hydrogel at different Gd(III) concentrations in DPBS at pH 7.4.

4. *In vivo* monitoring of non-labeled and Gd-labeled HA hydrogels after intracerebral injection in healthy rats

After the initial studies *in vitro*, we assessed the feasibility of long-term *in vivo* monitoring of the HA-GdDOTA hydrogel fate during several weeks after intracerebral injection (10 µL) in healthy rats (n = 9) with T_1-MRI. Hydrogels were scanned with T_1-weighted imaging (T_1W) and quantitative T1 mapping sequences to determine the image features and relaxation times, respectively.

T_2-weighted (T_2W) imaging was also conducted to monitor the fate of the HA-GdDOTA hydrogel as well as the HA-ref scaffold which was injected as a control in the contralateral hemisphere. Indeed, the hydrogels can also be visualized with T_2-MRI at the injection site in healthy rat brains. Both hydrogels were successfully administered in the rat striatum as only one injection among the 18 ones failed (one of the HA-ref hydrogel).

As can be seen from the MR images in Figure 6A the HA-GdDOTA hydrogel could be readily visualized by T_1 imaging. The Gd labeling was found to be stable over a period of 31 days in about half of the rats investigated (n = 4). Partial or full hydrogel elimination was observed in the same time-lapse following administration in the other rats (n = 5). It can be noted that elimination started 14 days after implantation. In contrast, the HA-ref hydrogel, which is not detectable by T_1-MRI, was still present in all rats (n = 8) after 31 days in T_2 MR images.

For each individually segmented rat brain, we computed the mean T1 values for the implanted hydrogels over the period of 31 days. Figure 6B shows that the T_1 value is on average 3-fold lower for the Gd-labeled HA hydrogel than for the non-labeled one. The T_1 values of the latter hydrogel measured at day 2 ($2.0 < T1\ (s) < 3.5$) are in good agreement with the T_1 value of the HA-ref hydrogel phantom (T_1 = 2.3 s, Figure 5C). With regard to the T_1 values of the HA-GdDOTA hydrogel at day 2 ($0.6 < T_1\ (s) < 0.95$), they are slightly higher than that of the HA-GdDOTA hydrogel phantom (T_1 = 0.19 s, Figure 5C) in which the Gd(III) concentration is slightly higher (0.65 *in vitro* versus 0.61 mM *in vivo*).

It can be noted that for mean T_1 values of both hydrogels, the largest dispersion is for the Gd-labeled HA hydrogel 14 days following implantation. This correlates with the elimination of the hydrogel in about half of the rats.

The volumes of hydrogels (V_{gel}) after implantation were also measured from the T_2W images as a function of time (Figure 6C). The volumes determined for the HA-ref hydrogel are between 9.4 et 11.3 μL, which is in good agreement with the injected volume (10 μL). Similar values are obtained for the HA-GdDOTA hydrogel ($10.0 < V_{gel}$ (μL) < 12.1). There was a progressive decline of the HA-ref hydrogel volumes over time and at day 31, the volumes are between 6.6 and 9.9 μL. The trend was different for the HA-GdDOTA hydrogel. Indeed, the volumes progressively decreased similar to the HA-ref hydrogel for 4 rats while a sharp diminution was noticed for the other 5 rats ($3.9 < V_{gel}$ (μL) < 6.7 at day 31). As mentioned above, the hydrogel in these rats was hardly detectable by T_1 imaging at day 31.

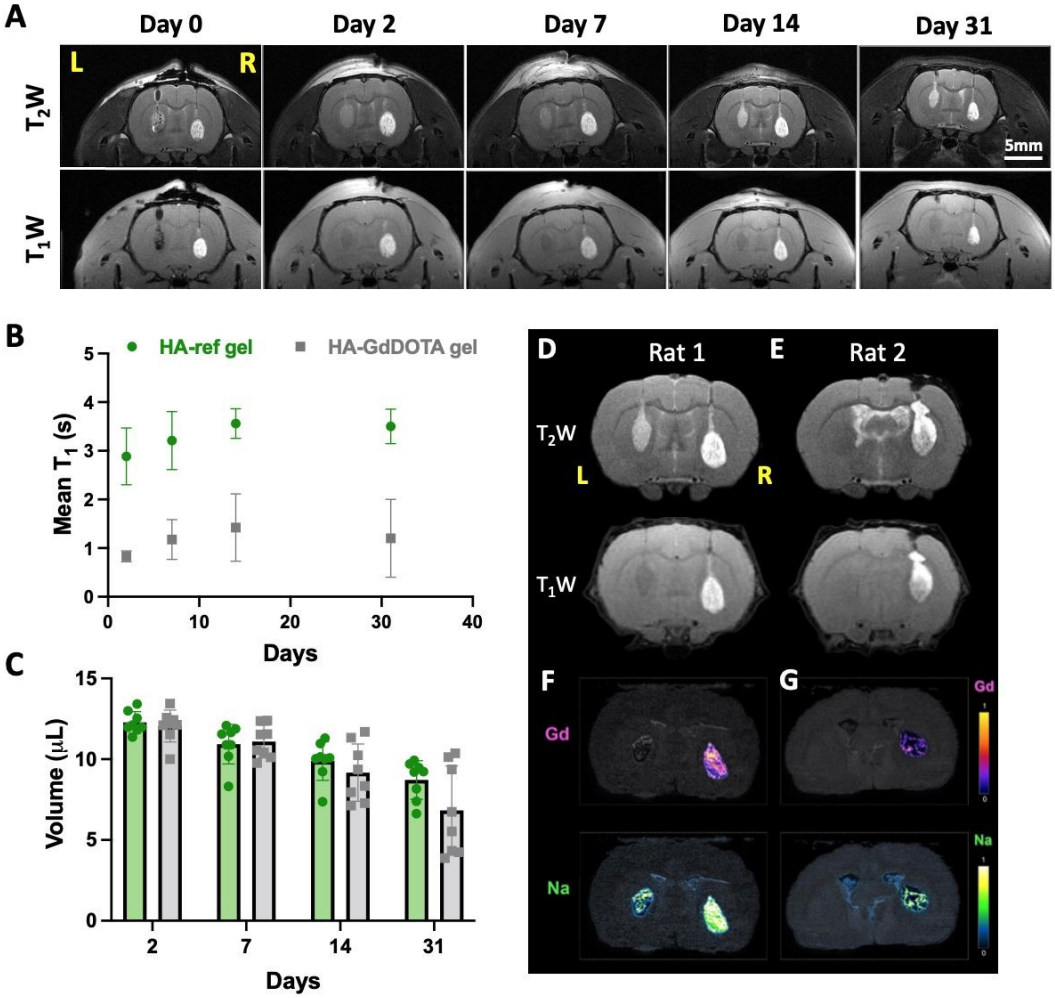

Fig. 6 *In vivo* monitoring of the HA-ref and HA-GdDOTA hydrogels with T_1 and T_2-MRI at 4.7 T after intracerebral injection in healthy rats (n = 9). A) Representative T_1W and T_2W MR images of a rat brain transplanted with both hydrogels; left (L): HA-ref hydrogel, and right (R): HA-GdDOTA hydrogel ($[Gd^{3+}] = 0.61$ mM). B) Mean T_1 values for the implanted HA-ref and HA-GdDOTA hydrogels; note that at day 31, the T_1 values for the HA-GdDOTA hydrogel were measured only in rats where it was still detected by T_1 MRI (n = 5). C) Volumes of the HA-ref and HA-GdDOTA hydrogels measured from the T_2W images of brains of rats (n = 8). D,E) MR images at day 31 and, F,G) *ex vivo* LIBS elemental images of two rat brains. Images at left show successful injection of the HA-ref hydrogel (L) and HA-GdDOTA hydrogel (R) in rat 1 (same animal as in A); images at right show failed injection of the HA-ref hydrogel (L) in rat 2. The LIBS elemental images show the presence of Gd in both brains, which is in line with the high signal intensity observed on T_1W MR images (R). LIBS elemental images have been recorded with a spatial resolution of 40 μm.

The presence of Gd from the HA hydrogel implanted in the brain was confirmed by LIBS analyses post-mortem. LIBS has demonstrated its effectiveness as a powerful tool for building up elemental chemical maps of biological tissues.[45] The LIBS images (Figure 6F and 6G) show the presence of Gd in both rat brains, which is in line with the high signal intensity observed on the T_1W MR images on day 31 (Figure 6D and 6E). Worthy of note is that analysis of Na by LIBS could also confirm the presence of the HA-ref hydrogel in the contralateral hemisphere in rat 1 (Figure 6F and 6D). Since Na ions are likely from HA which contains sodium ions as the carboxylate counterions, Na was found to be co-localized with Gd in the hemisphere of rats which received the HA-GdDOTA hydrogel. All together, these data demonstrate stability of the Gd(III) labeling of the HA hydrogel up to one month after intracerebral injection.

5. Host response to implanted hydrogels

Following the final imaging at 31 days post-injection, cerebral tissues were harvested and analyzed to locate the

View Article Online
DOI: 10.1039/D4TB02722A

hydrogel and its injection sites (correlating with imaging data) and to assess the tissue response to the intracerebral hydrogel. Hematoxylin and eosin (HE) staining enabled visualization of the injection sites and did not indicate pronounced cellular hyperlocalization around these sites, suggesting the absence of an intense tissue reaction following the injections (Figure 7A, 7B1, 7C1).

Cresyl violet (CV) staining demonstrated high affinity and specificity for the hyaluronic acid component within the hydrogel, thereby enabling visualization of the hydrogel scaffold post-transplantation. At 31 days post-injection, the gel was not fully degraded within the healthy tissue, as evidenced by the intense staining observed at the injection sites. This staining corresponds to the dehydrated hydrogel, resulting from various dehydration treatments required for staining (Figure 7A, 7B2, 7C2). At the final imaging time point on day 31 post-injection in healthy rat brains, GFAP+ astrocytes were detected around the hydrogel scaffold injection site. Immunohistochemical analysis of GFAP-stained tissue sections revealed that both control and modified gels were associated with low-grade gliosis in the adjacent host tissue. Specifically, regardless of the presence of Gd in the hydrogel, GFAP+ astrocytes were localized at the periphery of the hydrogel, forming a glial scar approximately 20 µm thick (with a maximum of two cell layers in certain regions). The gliosis had developed at and around the hydrogel-brain interface and was characterized by tightly packed GFAP-positive astrocytes and processes (Figure 7D1). Staining for astrocytic scarring (GFAP) and microglial activation (Iba-1) (Figure 7D2 and Figure S5) revealed no significant differences in the inflammatory response following gel injection between the two conditions. Furthermore, Iba-1+ cells surrounding the injection site displayed a stellate morphology, suggesting the presence of resting microglia. This mild tissue response was also associated with an absence of reactive peripheral neoangiogenesis, as evidenced by ColIV staining (Figure 7B4, 7C4).

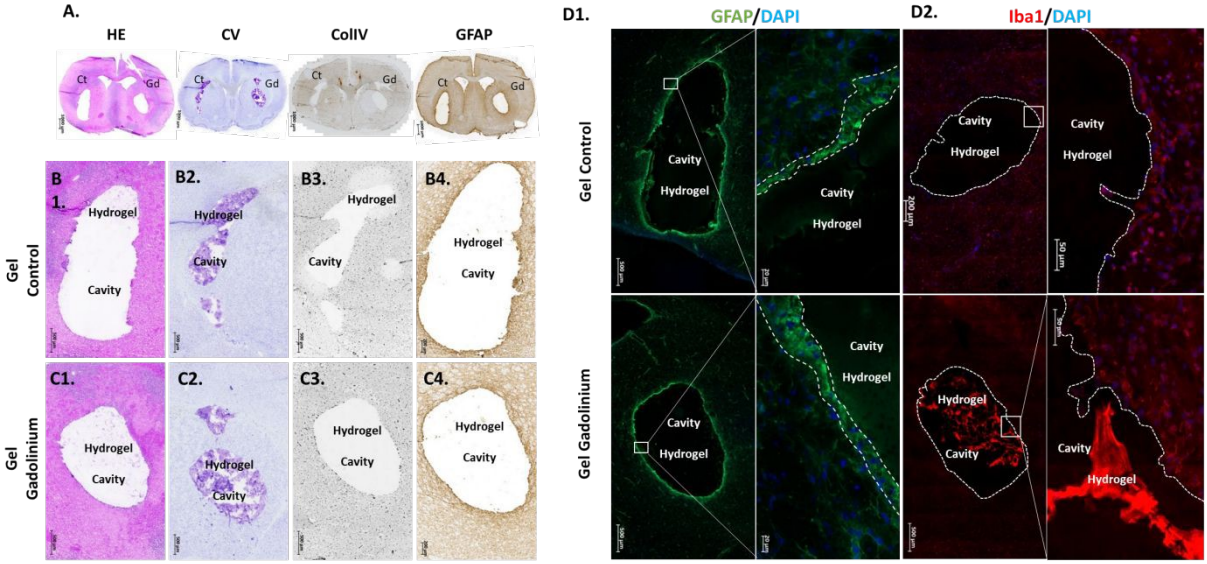

Fig. 7 Host response to implanted hydrogel for endogenous in situ brain tissue engeneering. A) Macroscopic visualization of brain tissue reaction and hydrogels after implantation by hematosin-eosin (HE), cresyl violet (CV), Collagen-IV (ColIV) and GFAP stainings. Histological assessment at day 31 after steraotaxic transplantation into healthy rat brain using HE-CV staining, in which the scaffold appears purple. The lesion cavity is defined by glial scarring (GFAP). Immunchemistry staining of vessels (ColIV) in the brain after hydrogels implantation do not reveal proangiogenic reactivity (Ct= control hydrogel; Gd= Gadolinum hydrogel). B. and C. Image enlargements of histologic stainings reveal the injection cavity and the tissue reactivity for the control hydrogel (B1-4) and Gadolinium hydrogel (C1-4). D1. Glial scarring. A histological comparison between control and gadolinium hydrogels 31 days after implantation reveal a small increase in GFAP staining at the border of the cavity. D2. Immunofluorescence staining of microglia (Iba1) in the brain after hydrogels implantation. Blue, DAPI; Green GFAP; Red, Iba1.

6. MR imaging of the hydrogel after intracerebral injection in a rat model of stroke

At 6 days post-induction, volumetric MRI comparison of lesion volumes prior to implantation of hydrogel showed no lesion in one animal and lesion volumes ranging from 10 to 43 µL in the other three animals. Upon hydrogel injection (10 µL) into the lesion core, a T_1W signal covering the damaged area (T_2W signal) was evident post-injection in 2 of the 3 animals (Figure 8A). The hydrogel could thus be successfully injected at the target site in animals with the highest lesion volumes pre-implantation (26 and 43 µL). In these animals, the signal in the T_1W images due to the hydrogel dramatically decreased within the first 4 days post-implantation to reach nearly baseline levels 11 days following injection (at 17-days post-stroke). As seen from Figure 8B, the T_1 value of hydrogel increased over time in both rat brains to reach a value of 3.4 and 4.3 s at 17-days post-stroke. The latter values are of the same order of magnitude of the T_1 values measured at day 6 before hydrogel injection ($T_1 = 3.6 \pm 0.56$ s). The gradual increase in T_1 can be attributed to a decrease in the

View Article Online
DOI: 10.1039/D4TB02722A

hydrogel's density and to the removal of Gd-chelate along with the hydrogel degradation products .

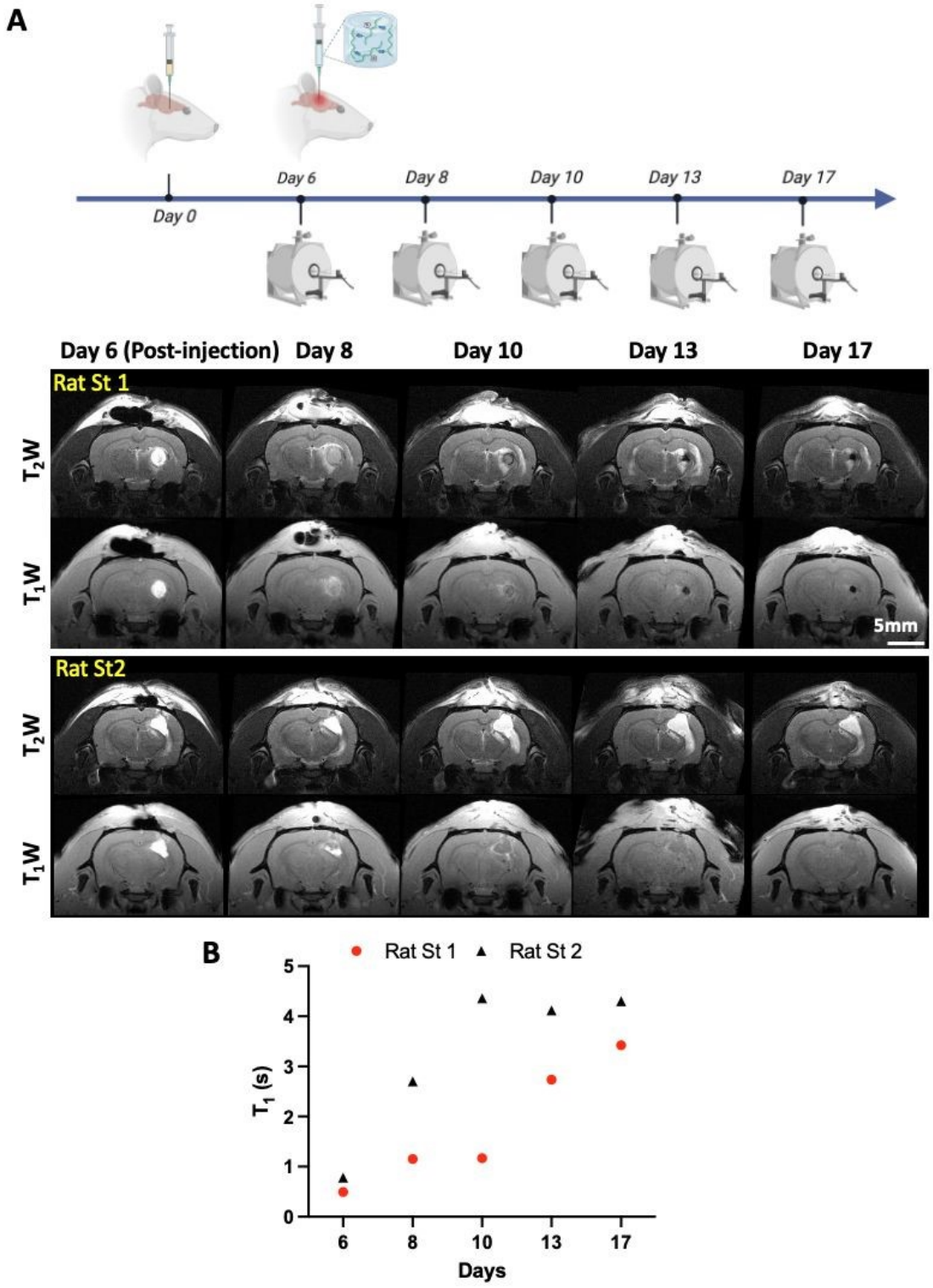

Fig. 8 *In vivo* monitoring of the HA-GdDOTA hydrogel with T1 and T2-MRI at 4.7 T after intracerebral injection in 2 rats at 6-days post-stroke. A) T1w and T2w MR images of both rat brains transplanted with the HA-GdDOTA hydrogel. B) T1 values for the implanted HA-Fru-GdDOTA hydrogel.

Discussion

In recent years, self-healing hydrogels have received much attention in tissue regeneration and cell delivery.[46-50] Studies in animal models showed their potential for treating brain disorders when used alone or as cell/drug carriers.[51] However, their efficacy was determined by examining indirect parameters such as brain tissue repair or functional recovery, and none of these studies elucidated further on the retention and behavior of the hydrogel at the target site

View Article Online
DOI: 10.1039/D4TB02722A

over a long time span. This lack of information makes it difficult to link the hydrogel content *in vivo* to the therapeutic effect.[52]

In this study, we developed an injectable self-healing HA hydrogel labeled with a T_1 MRI contrast agent for monitoring delivery and retention in the brain. The hydrogel demonstrated outstanding mechanical properties, exceptional elasticity and favorable biocompatibility. The biocompatibility of the hydrogel was validated *in vitro* through cell viability assays conducted on hASCs.

HA was utilized to synthesize the hydrogel network as it is biocompatible, biodegradable and abundantly found in the brain. Some work showed favorable effects of HA scaffolding on engrafted cell survival in preclinical models of stroke.[53-55] However, the beneficial effect of cell-supporting HA hydrogel scaffolds is closely tied to the precision of injection, ability to fill irregular tissue defects and retention of the scaffold material within the tissue, which depend on the gelation properties of HA. Using chemical exchange saturation transfer (CEST)-MRI, Liang *et al.* showed the ability to monitor for several weeks the degradation of a covalently-crosslinked hydrogel based on gelatin and HA after transplantation in healthy mouse brains.[56] In this study, quantification of the scaffold degradation rate was realized by targeting the gelatin component because of its stronger CEST effect compared to HA. Herein, in order to specifically track *in vivo* HA, the only biopolymer component of our hydrogel, we used a different approach based on tethering to HA a Gd-based contrast agent that generates T_1 contrast. Previous studies have reported the preparation of injectable HA hydrogels modified with a linear-type Gd-chelate agent (Gd−diethylenetriaminepentaacetic acid (DTPA))[18] and a dendronized HA derivative containing cyclic Gd-chelates (Gd-tetraazacyclododecane-1,4,7,10-tetraacetic acid (DOTA))[57]. In the latter compound, DOTA was grafted to the dendron through amide bond formation with one of its carboxylic acids. However, the change of a coordinating carboxylate to an amide dramatically reduces the stability of the Gd-DOTA complex by ca. 10^5-fold.[58] The resulting value becomes even lower than that of Gd-DTPA, whose clinical use is currently prohibited or is not recommended in many countries due to its low Gd-chelating stability.[34, 58]

Therefore, in the present work, we modified HA with a GdDOTA-like complex which still contains four coordinating carboxylates after its conjugation to HA. Chelation of Gd(III) to a thermodynamically stable and kinetically inert complex grafted to HA was a fundamental requirement for specifically monitoring the long-term fate of our HA hydrogel after intracerebral administration. After injection in healthy rat brains, the HA-GdDOTA hydrogel could be readily visualized by T_1 MRI up to 31 days, showing stability of the Gd Labeling. This was confirmed by post-mortem LIBS analyses which demonstrated co-localization of Na ions from HA and Gd. To the best of our knowledge, this is the first study showing ability to detect Gadolinium by LIBS in brain tissue. Moreover, although T_2W imaging itself is not specific for the hydrogel as the signal is derived from unbound water protons in the hydrogel, the volumetric changes calculated from the T_2W images, revealing a progressive decrease of hydrogel volume over time, were found to be consistent with the increase of the mean T_1 value observed from day 14 post-administration. At this time point, the Gd-labeled hydrogel elimination was seen in 5 of out the 9 rats, while hydrogel was only partially eliminated in the other animals. It could indeed still be detected at day 31. The unmodified hydrogel, or the hydrogel conjugated with Gd, exhibited good biocompatibility *in vivo* within the central nervous system. Indeed, its implantation in healthy tissue did not provoke a significant reaction in the cerebral tissue. Indeed, the gel induced only a minimal tissue response, characterized by weak cellular accumulation around the gel and a low glial and microglial reaction. The positive *in vitro* and *in vivo* results further encourage the exploration of combining the hydrogel with stem cells as a promising direction for future research.

Interestingly, the Gd-labeling of the hydrogel enabled a selective visualization of its distribution in the lesion core after stroke. T_1W MRI revealed higher degradation kinetics of the HA network in the hostile stroke microenvironment compared to healthy brain. It is important to note that the hydrogel was injected within the acute stroke phase, which is characterized by rapid cell death, and infiltration of immune cells whose job is partly to clear cellular and matrix debris in the damaged area[31]. In spite of these conditions, the HA hydrogel remained visible by T_1W MRI up to 4 days post-implantation. Previous studies showed that extracellular matrix (ECM) hydrogels implanted in the lesion cavity at 14-days post-stroke underwent degradation at rates varying from 2.5 to 6.1 μL/day depending on hydrogel concentration.[59] Considering the injected volume (10 μL) and the residence time of our HA hydrogel, it can be inferred that its degradation rate is of the same order of magnitude, in spite of the different time window of implantation. Indeed, the ECM hydrogels were implanted in a post-stroke period during which the immune response shifts from a pro-inflammatory to a pro-repair environment.[60, 61]

Conclusion

In this study, we designed and characterized a novel Gd-labeled injectable self-healing HA hydrogel as a T_1 MRI-detectable scaffolding candidate for treating brain disorders, such as stroke. Our data demonstrated the ability to selectively monitor the fate of the hydrogel in healthy rat brains for up to 31 days by MRI. The HA network did not induce adverse tissue response and was biocompatible with therapeutic cells. Indeed, the hydrogel architecture was conducive to cell survival *in vitro*. Importantly, the labeling strategy was shown to be effective for tracking the distribution and degradation of hydrogel in stroke conditions, allowing a better assessment of efficacy and safety. It could enable the detection of differences in the degradation rate of the injected scaffolds through T_1 measurements. This must be confirmed in further larger studies. This MRI visible hydrogel thus appears as a promising candidate as scaffold that can be loaded with stem cells, growth factors and/or drugs for achieving effective treatments for brain disorders.

Data availability

The data supporting this article have been included as part of the ESI.†

Author contributions

View Article Online
DOI: 10.1039/D4TB02722A

M.S. and J. J.: investigation, writing – original draft. O.M.: MRI experiments and data analyses. N.C:. Cell and animal experiments and B.E.A.: MRI acquisitions. F.V.: histological examinations. B.C., I. J., B. L.: validation – review & editing. E.L.B.: methodology – review & editing. O.D.: conceptualization, validation – review & editing, supervision. C.R.: conceptualization, validation, writing – review & editing, supervision, project administration. R.A.: conceptualization, validation, writing – review & editing, supervision, project administration, funding acquisition. All authors discussed and revised the paper.

Conflicts of interest

There are no conflicts to declare.

Acknowledgements

This project was funded by the French organization "Fondation pour la Recherche Médicale" (DCM20181039533), and partly funded by the French national research agency (ANR18-CE19-003, Breakthru grant). ANR also supported the national infrastructure: " E-Cell France "The national research infrastructure for regenerative medicine - MSC-based therapies" (France 2030 / ANR-24-INBS-003)). The authors would like to acknowledge Grenoble MRI facility IRMaGe, partly funded by the French program "Investissement d'Avenir" run by ANR (ANR-11-INBS-0006) for the MRI 4.7T measurements; the NMR platform of ICMG (FR2607) for its support; and StrokeLink: F-CRIN French network for stroke research.

References

1. E. Hasanzadeh, A. Seifalian, A. Mellati, J. Saremi, S. Asadpour, S. E. Enderami, H. Nekounam and N. Mahmoodi, *Materials Today Bio*, 2023, **20**, 100614.
2. M. A. Grimaudo, G. S. Krishnakumar, E. Giusto, F. Furlani, G. Bassi, A. Rossi, F. Molinari, F. Lista, M. Montesi and S. Panseri, *Acta Biomater.*, 2022, **140**, 88-101.
3. P. H. Lin, Q. Dong and S. Y. Chew, *Mater Adv*, 2021, **2**, 2561-2583.
4. B. Niemczyk, P. Sajkiewicz and D. Kolbuk, *Journal of Neural Engineering*, 2018, **15**, 051002.
5. L. R. Nih, S. T. Carmichael and T. Segura, *Curr Opin Biotechnol*, 2016, **40**, 155-163.
6. M. Modo, *Front Neurosci*, 2019, **13**, 1156.
7. Z. Z. Khaing, R. C. Thomas, S. A. Geissler and C. E. Schmidt, *Materials Today*, 2014, **17**, 332-340.
8. M. N. Collins, F. Zamboni, A. Serafin, A. Escobar, R. Stepanian, M. Culebras, R. L. Reis and J. M. Oliveira, *In vitro models*, 2022, **1**, 129-150.
9. G. Jensen, J. A.-O. Holloway and S. E. Stabenfeldt, *Cells*, 2020, **9**, 2113.
10. Y. C. Dong, M. Bouche, S. Uman, J. A. Burdick and D. P. Cormode, *ACS Biomater. Sci. Eng.*, 2021, **7**, 4027-4047.
11. J. Liu, K. Wang, J. Luan, Z. Wen, L. Wang, Z. Liu, G. Wu and R. Zhuo, *J Mater Chem B*, 2016, **4**, 1343-1353.
12. K. Ohno, L. Samaranch, P. Hadaczek, J. R. Bringas, P. C. Allen, V. Sudhakar, D. E. Stockinger, C. Snieckus, M. V. Campagna, W. San Sebastian, J. Naidoo, H. Chen, J. Forsayeth, E. A. Salegio, G. G. C. Hwa and K. S. Bankiewicz, *Mol Ther Methods Clin Dev*, 2019, **13**, 47-54.
13. P. Walczak, J. Wojtkiewicz, A. Nowakowski, A. Habich, P. Holak, J. Xu, Z. Adamiak, M. Chehade, M. S. Pearl, P. Gailloud, B. Lukomska, W. Maksymowicz, J. W. M. Bulte and M. Janowski, *J Cereb Blood Flow Metab*, 2016, **37**, 2346-2358.
14. J. Wahsner, E. M. Gale, A. Rodríguez-Rodríguez and P. Caravan, *Chem Rev*, 2019, **119**, 957-1057.
15. M. Moon, R. G. Thomas, S. U. Heo, M. S. Park, W. K. Bae, S. H. Heo, N. Y. Yim and Y. Y. Jeong, *Mol Imaging Biol*, 2015, **17**, 497-503.
16. R. Buffa, J. Betak, S. Kettou, M. Hermannova, L. Pospisilova and V. Velebny, *Carbohydr Res*, 2011, **346**, 1909-1915.
17. M. H. Bakker, C. C. S. Tseng, H. M. Keizer, P. R. Seevinck, H. M. Janssen, F. J. Van Slochteren, S. A. J. Chamuleau and P. Y. W. Dankers, *Adv Healthc Mater*, 2018, **7**, e1701139.
18. D. Bermejo-Velasco, W. Dou, A. Heerschap, D. Ossipov and J. Hilborn, *Carbohydr Polym*, 2018, **197**, 641-648.
19. M. Weerasekare, M. B. Taraban, X. Shi, E. K. Jeong, J. Trewhella and Y. B. Yu, *Biopolymers*, 2011, **96**, 734-743.
20. A. Berdichevski, H. Simaan Yameen, H. Dafni, M. Neeman and D. Seliktar, *Proc. Natl Acad. Sci. USA*, 2015, **112**, 5147-5152.
21. K. Lei, Q. Ma, L. Yu and J. Ding, *J Mater Chem B*, 2016, **4**, 7793-7812.
22. P. Hermann, V. Kotek J Fau - Kubícek, I. Kubícek V Fau - Lukes and I. Lukes, *Dalton Trans.*, 2008, 3027-3047.
23. D. Tarus, L. Hamard, F. Caraguel, D. Wion, A. Szarpak-Jankowska, B. van der Sanden and R. Auzely-Velty, *ACS Appl. Mater. Interfaces*, 2016, **8**, 25051-25059.
24. T. Figueiredo, J. Jing, I. Jeacomine, J. Olsson, T. Gerfaud, J.-G. Boiteau, C. Rome, C. Harris and R. Auzély-Velty, *Biomacromolecules*, 2020, **21**, 230-239.
25. E. Brücher, in *Contrast Agents I: Magnetic Resonance Imaging*, ed. W. Krause, Springer Berlin Heidelberg, Berlin, Heidelberg, 2002, pp. 103-122.
26. J.-M. Idée, M. Port, C. Robic, C. Medina, M. Sabatou and C. Corot, *Journal of Magnetic Resonance Imaging*, 2009, **30**, 1249-1258.
27. K. Overoye-Chan, S. Koerner, R. J. Looby, A. F. Kolodziej, S. G. Zech, Q. Deng, J. M. Chasse, T. J. McMurry and P. Caravan, *J Am Chem Soc*, 2008, **130**, 6025-6039.
28. A. Barge, G. Cravotto, E. Gianolio and F. Fedeli, *Contrast Media Mol Imaging*, 2006, **1**, 184-188.
29. T. Figueiredo, V. Cosenza, Y. Ogawa, I. Jeacomine, A. Vallet, S. Ortega, R. Michel, J. D. M. Olsson, T. Gerfaud, J.-G. Boiteau, J. Jing, C. Harris and R. Auzély-Velty, *Soft Matter*, 2020, **16**, 3628-3641.
30. P. Cayot and G. Tainturier, *Anal Biochem*, 1997, **249**, 184-200.
31. O. Detante, L. Legris, A. Moisan and C. Rome, *Neuroscience*, 2024, **550**, 79-88.
32. C. Cirillo, A. Le Friec, I. Frisach, R. Darmana, L. Robert, F. Desmoulin and I. Loubinoux, *Front Neurol*, 2018, **9**, 1072.
33. D. Milford, N. Rosbach, M. Bendszus and S. Heiland, *PLOS ONE*, 2015, **10**, e0145255.
34. P. Caravan, J. J. Ellison, T. J. McMurry and R. B. Lauffer, *Chem Rev*, 1999, **99**, 2293-2352.
35. V. Kubíček, J. Havlíčková, J. Kotek, G. Tircsó, P. Hermann, É. Tóth and I. Lukeš, *Inorganic Chemistry*, 2010, **49**, 10960-10969.

View Article Online
DOI: 10.1039/D4TB02722A

36. C. Bernhard, M. Moreau, D. Lhenry, C. Goze, F. Boschetti, Y. Rousselin, F. Brunotte and F. Denat, *Chem Eur J*, 2012, **18**, 7834-7841.
37. N. Sahiner, E. Umut, S. S. Suner, M. Sahiner, M. Culha and R. S. Ayyala, *Carbohydr Polym*, 2022, **277**, 118873.
38. S. Kadi, D. Cui, E. Bayma, T. Boudou, C. Nicolas, K. Glinel, C. Picart and R. Auzély-Velty, *Biomacromolecules*, 2009, **10**, 2875-2884.
39. E. Axpe, G. Orive, K. Franze and E. A. Appel, *Nature Commun.*, 2020, **11**, 3423.
40. Z.-J. Chen, G. T. Gillies, W. C. Broaddus, S. S. Prabhu, H. Fillmore, R. M. Mitchell, F. D. Corwin and P. P. Fatouros, *J Neurosurg*, 2004, **101**, 314-322.
41. R. Pomfret, G. Miranpuri and K. Sillay, *Ann. Neurosci.*, 2013, **20**, 118-122.
42. S. Besse, PhD Thesis, Université de Grenoble, 2010.
43. S. Laurent, L. V. Elst and R. N. Muller, *Contrast Media Mol Imaging*, 2006, **1**, 128-137.
44. A. M. Ponsiglione, M. Russo, P. A. Netti and E. Torino, *Interface Focus*, 2016, **6**, 20160061.
45. L. Sancey, V. Motto-Ros, B. Busser, S. Kotb, J. M. Benoit, A. Piednoir, F. Lux, O. Tillement, G. Panczer and J. Yu, *Scientific Reports*, 2014, **4**, 6065.
46. P. Bertsch, M. Diba, D. J. Mooney and S. C. G. Leeuwenburgh, *Chem Rev*, 2023, **123**, 834-873.
47. T. Kikani, S. Dave and S. Thakore, *Int. J. Biol. Macromol.*, 2023, **242**, 124950.
48. S. Talebian, M. Mehrali, N. Taebnia, C. P. Pennisi, F. B. Kadumudi, J. Foroughi, M. Hasany, M. Nikkhah, M. Akbari, G. Orive and A. Dolatshahi-Pirouz, *Adv. Sci.* , 2019, **6**, 1801664.
49. Y. Tu, N. Chen, C. Li, H. Liu, R. Zhu, S. Chen, Q. Xiao, J. Liu, S. Ramakrishna and L. He, *Acta Biomater.*, 2019, **90**, 1-20.
50. S. Wang, S. Tavakoli, R. P. Parvathaneni, G. N. Nawale, O. P. Oommen, J. Hilborn and O. P. Varghese, *Biomater. Sci.*, 2022, **10**, 6399-6412.
51. J. Xu and S.-h. Hsu, *J. Biomed. Sci.*, 2023, **30**, 43.
52. M. J. G. Schotman and P. Y. W. Dankers, *Adv. Mater. Interf.*, 2022, **9**, 2100942.
53. P. Moshayedi, L. R. Nih, I. L. Llorente, A. R. Berg, J. Cinkornpumin, W. E. Lowry, T. Segura and S. T. Carmichael, *Biomaterials*, 2016, **105**, 145-155.
54. J. Samal and T. Segura, *Brain Res. Bull.*, 2021, **176**, 25-42.
55. J. Zhong, A. Chan, L. Morad, H. I. Kornblum, G. Fan and S. T. Carmichael, *Neurorehabil Neural Repair*, 2010, **24**, 636-644.
56. Y. Liang, P. Walczak and J. W. M. Bulte, *Biomaterials*, 2013, **34**, 5521-5529.
57. C. Guo, L. Sun, H. Cai, Z. Duan, S. Zhang, Q. Gong, K. Luo and Z. Gu, *ACS Appl. Mater. Interfaces*, 2017, **9**, 23508-23519.
58. M. Yokoyama and K. Shiraishi, *Magn. Reson. Mater. Phys. Biol. Med.*, 2020, **33**, 527-536.
59. H. Ghuman, C. Mauney, J. Donnelly, A. R. Massensini, S. F. Badylak and M. Modo, *Acta Biomater.*, 2018, **80**, 66-84.
60. C. Damian, H. Ghuman, C. Mauney, R. Azar, J. Reinartz, S. F. Badylak and M. Modo, *Int J Mol Sci*, 2021, **22**.
61. J. Lyu, D. Xie, T. N. Bhatia, R. K. Leak, X. Hu and X. Jiang, *CNS Neurosci Ther.*, 2021, **27**, 515-527.

The authors confirm that the data supporting the findings of this study are available within the article and its supplementary materials.

View Article Online
DOI: 10.1039/D4TB02722A